Bicycle Simulator Improvement and Validation

Murad M Shoman, Hocine Imine

IEEE Access
Multidisciplinary | Rapid Review | Open Access Journal

Date of publication xxxx 00, 0000, date of current version xxxx 00, 0000.

Digital Object Identifier 10.1109/ACCESS.2017.DOI

Bicycle Simulator Improvement and Validation

MURAD M. SHOMAN[1], and HOCINE IMINE[2]

[1]Laboratoire sur la Perception, les Interactions, les Comportements et la Simulation des usagers de la route et de la rue (PICS-L),Components and systems department (cosys), Gustave Eiffel University, Champs sur Marne, 77420 France (e-mail: murad.shoman@univ-eiffel.fr)
[2]same affiliation (e-mail: hocine.imine@univ-eiffel.fr)

Corresponding author: M. Shoman (e-mail: murad.shoman@univ-eiffel.fr).

This work is funded by Marie Skłodowska-Curie actions (H2020 MGA MSCA-ITN) within the SAFERUP project under grant agreement number 765057.

ABSTRACT In this paper, we present the new features implemented on the bicycle simulator developed by the Perceptions, Interactions, Behaviors and Simulations Lab for road and street users (PICS-L) at Gustave Eiffel University. The added features were deemed necessary to study road-bicycle interactions. We equipped the simulator platform with: three actuators to render the road profile vibrations, an asphalt specimen attached to the rear tire to render the road adhesion, and a new virtual reality environment to render a part of the city of Vanves in France. Simultaneously, we developed a mathematical model with 6 degrees of freedom including the three rotational angles (Yaw, Pitch and Roll) and their influence on vertical, lateral and longitudinal modeling. In order to validate the simulator and the developed model physically and subjectively, we conducted an experiment involving 36 participants who rode the simulator for around 600 meters with full control on the handlebar, pedals and brakes. The improved simulator/mathematical model will be employed to further study bicycle dynamics, cyclist behavior and the interaction with the infrastructure and other road users.

INDEX TERMS Bicycle Modeling, Bicycle Simulator,Experimental Validation, Road characteristics, Simulation.

I. INTRODUCTION

THIS paper is an extended version of our previous work on modeling and simulation of bicycle dynamics published in [1] and on subjective validity of bicycle simulators published in [2]. Hereinafter, we present more details on the recent developments of the simulator and the underlying mathematical model, as well as its physical and subjective experimental validation.

Experimentation in real environment is not always the appropriate means, due to its costs, bias related to uncontrolled variables and risks facing cyclists [3] [4] [5] [6] [7]. On the contrary, simulators allow to detect the behavior of cyclists and other road users in various riding situations, while controlling the variables at play and avoiding the risks associated with a real environment [8]. However, simulator studies are valid insofar as: 1) providing results that can be generalized to real-world situations; 2) minimizing the occurrence of unwanted symptoms that may result from motion or exposure to the virtual environment (i.e. simulator sickness).

In order to model a vehicle (including a bicycle), researchers deployed the theoretical physical approach, such as Lagrange, Euler equations or the detailed nonlinear Whipple scientific description [9] [10]; for example, [11] used the Linear–quadratic regulator (LQR algorithm) to analyze the bicycle mathematical model, this method is considered accurate but time-consuming at the same time. For a straightforward and time efficient modeling, the classical single-track model could be an alternative [12].

Overall, bicycle simulators are designed to serve multiple purposes, such as training, sport, immersion in virtual reality, bicycle-dynamical modeling, and evaluation of cyclists' performance and behavior [13] [14] [15] [16] [17]. In PICS-L bicycle simulator, the single-track model was used to produce more convenient and accurate results that suit our research goals [18] [19] [20]. The simulator was developed to study the following environmental determinants of cyclists' behavior:

1) The environmental elements to which cyclists adapt their behavior (i.e. speed, safety gap, steering, etc.);
2) How cyclists adjust their riding practices as they inter-

This article has been accepted for publication in a future issue of this journal, but has not been fully edited. Content may change prior to final publication. Citation information: DOI 10.1109/ACCESS.2021.3071214, IEEE Access

act with other road users;

3) How cyclists anticipate risks in hazardous riding situations, and what strategies, equipment or behaviours they employ to cope with those risks;

Any road accident may result from the vehicle-user-infrastructure interaction [21] [22] [23], However, few studies have tackled the complex interaction between the three factors. The goal of this study was two-fold: to develop the mathematical model of the bicycle simulator dynamics, and to improve the simulator platform with the addition of vibration actuators to render the haptic feedback of a road profile (which gives more realistic feeling of cycling), and an asphalt specimen attached to the rear wheel to render road adhesion (which plays a key role when accelerating and braking). Furthermore, this will help to study the interaction between bicycles and road surface characteristics and geometries and their effect on cyclists' behavior. The long-term objective of this research is to improve cycling safety and foster the peaceful coexistence of cyclists and other road users in urban space; by taking into consideration the behavioral aspects in terms of bicycle control and similarity of behavior exhibited in real situations. The paper is structured as follows: the first section gives a brief overview of different bicycle models; the second part is devoted to bicycle modeling; the third part describes the experimentation and discusses the validation results:physically and subjectively; and we finalize with the conclusion and future work in the fourth part.

II. BICYCLE MODELING

The bicycle mathematical model (designed by using Simulink-Matlab from Mathworks) aims to reproduce the dynamics of a bicycle (in simulation or in a real environment). The simulator system allows to log the simulation data and the actions of the cyclist on handlebar, brake levers and derailleurs. Fig. 1 shows the operating flow of the bicycle simulator and the interaction between its different parts.

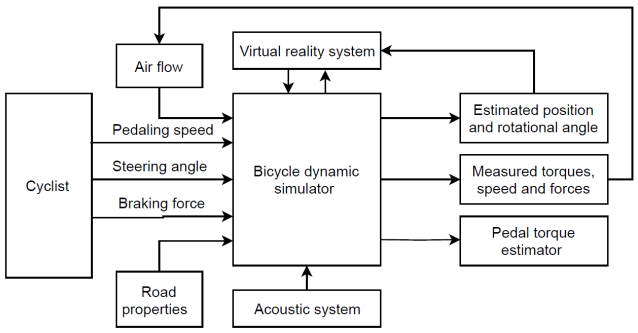

FIGURE 1. Operating flow of the bicycle simulator.

A. VERTICAL MODELING

The geometrical and mass parameters of the bicycle are divided as follows: the front part includes the steering axis, the front fork, the front wheel and a fraction of the cyclist mass; and the rear part includes the frame, the rear wheel and the other fraction of the cyclist body mass. The reactions of total mass are modelled by springs representing the tires stiffness (k_F and k_R) and damping coefficients (B_F and B_R). The bicycle has no suspension system. The fractions of the bicycle-rider-bicycle-rider-system mass are m_F and m_R. The tire contact, road profile, road adhesion, and radius of curvature are considered inputs of the system. The road profile is represented by the variable u. The pitch angle effect is neglected [24] [25]. Fig. 2 shows the main parameters used in the dynamical model of the simulator .

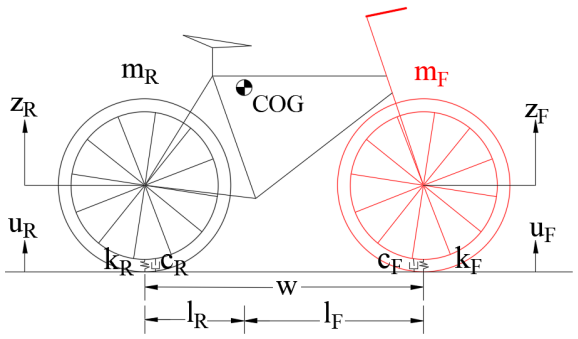

FIGURE 2. Side view of the bicycle model shows the geometrical and dynamical parameters of the bicycle used in the mathematical model. The model is divide into two parts: the front part (red) and the rear part (black).

The vertical acceleration values of the wheels ($\ddot{z}$) are obtained using (1) and (2):

$$\ddot{z}_F = \frac{k_F(u_F - z_F) - B_F\,\dot{z_F} - k_F\,l_R\,sin\phi}{m_F} \tag{1}$$

$$\ddot{z}_R = \frac{k_R(u_R - z_R) - B_R\,\dot{z_R} - k_R\,l_F\,sin\phi}{m_R} \tag{2}$$

where m_F and m_R are the masses of the front and rear parts, k_F and k_R are the front and rear tire vertical stiffness, B_F and B_R are the damping coefficients of the front and rear wheel, z_F and z_R are the vertical displacements of the Center of Gravity (COG) of the front and rear parts respectively, u_F and u_R are the front and rear values of road profile.
To obtain the vertical displacements z_F and z_R we integrated the acceleration twice. The normal forces F_{nF} and F_{nR} acting on the wheels are calculated in (3) and (4):

$$F_{nF} = F_{cF} + k_F(u_F - z_F) + B_F(\dot{u_F} - \dot{z_F}) \tag{3}$$

$$F_{nR} = F_{cR} + k_R(u_R - z_R) + B_R(\dot{u_R} - \dot{z_R}) \tag{4}$$

where F_{cF} and F_{cR} are the static forces of the bicycle-rider system applied to the front and rear wheel. They were calculated by applying the equilibrium equation. Assuming the bicycle-rider mass equals 85 kg, F_{cF} and F_{cR} are 230 and 630 N, respectively.

B. LATERAL MODELING

In order to calculate the lateral forces, it is necessary to know the tire slip, the side slip angle and the road adhesion coefficient.The tire side slip angle for both wheels were calculated using (5) and (6) then the lateral forces are calculated in (9) and (10)

$$\alpha_F = -\dot{\beta} + \delta_w - \frac{l_F\,\dot{\psi}}{v_{COG}} \tag{5}$$

$$\alpha_R = -\dot{\beta} + \frac{l_R\,\dot{\psi}}{v_{COG}} \tag{6}$$

where α_F and α_R are the side slip angles for the front and rear tires respectively, $\dot{\beta}$ is the velocity of the side slip angle at the COG, δ_w is the steering angle of the handlebar, l_F and l_R are distances from COG to front and rear axles, v_{COG} is the COG velocity, $\dot{\psi}$ is the yaw rate calculated using (7):

$$\dot{\psi} = \frac{V}{R_c} \tag{7}$$

V is the bicycle velocity and R_C is the radius of curvature calculated using (8):

$$R = \frac{l_f + l_r}{sin\delta_s} \tag{8}$$

where δ_s is the steering angle. The lateral forces for both front and rear wheel (considering the lateral slope of the road) are obtained using (9) and (10) :

$$F_{yF} = \alpha_F\,C_y + m_F\,g\,sin\phi \tag{9}$$

$$F_{yR} = \alpha_R\,C_y + m_R\,g\,sin\phi \tag{10}$$

where F_{yF} and F_{yR} are the lateral forces of the front and rear wheel respectively, C_y is the tire lateral stiffness and ϕ is the roll angle. The lateral acceleration of the bicycle simulator (a_y) is estimated using (11):

$$a_y = \frac{F_{yF} + F_{yR}}{m} \tag{11}$$

where m is the total mass of the bicycle-rider system. The double integration of the acceleration gives the lateral displacement.

C. LONGITUDINAL MODELING

The longitudinal frictional forces of front and rear wheels can be calculated from the adhesion coefficient using (12) and (13). This provides the frictional forces in the direction of the wheel ground contact velocity.

$$F_{xF} = \mu\,F_{zF}\,cos\alpha_F + F_{sF} + F_{aero} \tag{12}$$

$$F_{xR} = \mu\,F_{zR}\,cos\alpha_R + F_{sR} + F_{aero} \tag{13}$$

where F_{xF} and F_{xR} are the longitudinal forces for the front and rear wheel respectively, μ is the adhesion coefficient and F_{zF} and F_{zR} are the vertical forces applied on the front and rear wheels. F_{sF} and F_{sR} are the forces caused by the longitudinal slope of the road calculated using (14) and (15):

$$F_{sF} = m_F\,g\,sin\theta \tag{14}$$

$$F_{sR} = m_R\,g\,sin\theta \tag{15}$$

where θ is the road longitudinal slope.

The aerodynamic force resistance (F_{aero}) is calculated using (16):

$$F_{aero} = 0.5\,Cax\,\rho\,S\,v_x^2 \tag{16}$$

where C_{ax} is the coefficient of aerodynamic resistance given by the bicycle manufacturer, ρ is the air density in kg/m^3, S is the frontal surface area of the bicycle and the rider in m^2 and v_x is the longitudinal velocity.

D. ROTATIONAL MODELING

1) Yaw rotation

Yaw rotation modeling can be obtained by using the lateral forces as described in (17) :

$$\ddot{\psi} = \frac{F_{yF}\,l_f - F_{yR}\,l_r}{Izz} \tag{17}$$

where $\ddot{\psi}$ is the yaw angle acceleration, F_{yF} and F_{yR} are the lateral forces of the front and rear wheel and I_{zz} is the moment of inertia around z-axis. Yaw rate $\dot{\psi}$ was also calculated using (7). The yaw angle value is calculated by integrating the yaw rate.

2) Roll rotation

The roll angle about the bicycle's x-axis (ϕ) can be calculated using the speed and radius of curvature as in (**??**):

$$h\pi = \arctan(\frac{V^2}{g\,R_c}) \tag{18}$$

The roll acceleration ($\ddot{\phi}$) is calculated using the mass and rotation matrices [26] as in (19):

$$\ddot{\phi} = r_{31}\,\phi + r_{32}\,\delta + r_{34}\,v_x\,\dot{\psi} + r_{36}\,v_x\dot{\delta} - (m_{13}\,v_y + m_{23}\,\ddot{\psi} + m_{34}\,\ddot{\delta})/m_{33} \tag{19}$$

with

$$r_{31} = (m_F\,j + m_R\,h)g \tag{20}$$

where j and h are the vertical component of the center of gravity for the front and rear part of the bicycle respectively, and g is the gravitational acceleration.

$$r_{32} = m_F\,e\,g - \eta\,F_{zF} \tag{21}$$

This article has been accepted for publication in a future issue of this journal, but has not been fully edited. Content may change prior to final publication. Citation information: DOI 10.1109/ACCESS.2021.3071214, IEEE Access

where e is the perpendicular distance between the center of gravity of the front part and the fork and η is the bicycle trail.

$$r_{34} = -m_F\, j - m_R\, h - \frac{I_{yRF}}{R_F} - \frac{I_{yRR}}{R_R} \tag{22}$$

where I_{yRF} and I_{yRR} are the moments of inertia around the y-axis for the front and rear wheel respectively, R_f and R_r are the radii of front and rear wheel.

$$r_{36} = -\frac{I_{yRF}}{R_F\, cos\epsilon} \tag{23}$$

where ϵ is the bicycle caster angle (i.e. the angular displacement of the steering axis from the vertical axis of a steered wheel).

$$m_{13} = m_F\, j + m_R\, h \tag{24}$$

$$m_{23} = m_F\, j\, k - C_{xzGR} + (I_{zGF} - I_{xGF})\, sin\epsilon\, cos\epsilon \tag{25}$$

$$m_{33} = m_F\, j^2 + m_R\, h^2 + I_{xGR} + I_{xGF}\, cos\epsilon^2 + I_{zGF} sin\epsilon^2 \tag{26}$$

$$m_{34} = m_F\, e\, j + I_{zGF}\, sin\epsilon \tag{27}$$

The roll rate is calculated by integrating the roll acceleration.

3) Pitch rotation

The pitch angle acceleration of the bicycle body $\ddot{\theta}$ can be calculated depending on the stiffness of the tires as in (28):

$$\ddot{\theta} = -k_R\, l_r\, z_R + k_F\, l_f\, z_F + (k_R\, l_r - k_F\, l_f) z - (k_R\, l_r^2 - k_F\, l_f^2)\, sin\theta / I_{yy} \tag{28}$$

where I_{yy} is the moment of inertia around y-axis. The numerical values of the parameters are given in Appendix A.

III. EXPERIMENTAL VALIDATION

A. EXPERIMENTAL SETUP

The PICS-L bicycle simulator was built by placing a real bicycle on a static platform with one degree of freedom (the steering angle). In order to maximaize the immersion in the virtual reality, the simulator consists of several components (Fig. 3) which are:

1) A fan, placed in front of the bicycle, reproduces the airflow felt by cyclists in real situations. The fan speed is proportional to the rear wheel's speed.
2) Three actuators, installed on the platform, simulate the vibrations caused by the unevenness of the road surface. The acceleration is limited to +/- 1 g in order to keep the platform stable, the amplitude is limited to +/- 2.5 mm (up to +/- 5 mm) when the frequency is 10 Hz (up to 20 Hz).
3) An incremental encoder, attached to the fork, provides haptic force feedback to the handlebars and measures the steering angle and velocity.
4) A passive mechanical lateral suspension system allows participants to slightly tilt the bicycle when turning left or right.
5) A flywheel, attached to the rear wheel, simulates an inertia equal to 60 kg mass in actual cycling.
6) An incremental encoder calculates the speed of the rear wheel and increases the inertia up to 85 kg.
7) A cylindrical asphalt specimen in contact with the rear tire (installed recently to replace a plastic cylinder) simulates road adhesion. The specimen is made of hot mixed asphalt concrete. It is 10 cm in diameter and 12 cm in height, the specimen is penetrated in the center to allow a shaft of 2 cm diameter to pass along its axis for fixation (see Fig.4).

FIGURE 3. The PICSL-L bicycle simulator; the numbers represent some of the different features explained under the experimental setup section.

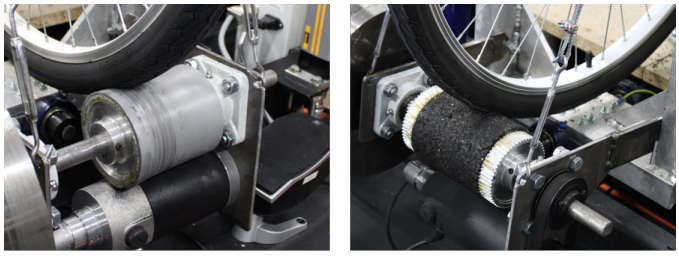

(a) (b)

FIGURE 4. Wheel-road surface interaction system (a) before and (b) after the installation of the asphalt specimen.

8) Five visual displays installed in front of the bicycle provide a visual angle of 225 degrees horizontally and 55 degrees vertically. A supplementary display device is placed behind the left shoulder of the cyclist for the rear visualisation of the road.

This article has been accepted for publication in a future issue of this journal, but has not been fully edited. Content may change prior to final publication. Citation information: DOI 10.1109/ACCESS.2021.3071214, IEEE Access

B. PARTICIPANTS

36 participants (18 male; mean age=28, SD=3.76 and 18 females; mean age=25.25, SD=2.06) participated in this experiment. All declared normal or corrected-to-normal vision. The mean cycling experience of the participants was 14.5 years. The average number of cycling kilometers per month was 20.6 km. Fig. 5 shows one of the participants during the familiarization phase of the experiment; the bus-bicycle shared lane, and the traffic on both sides.

FIGURE 5. A participant during the familiarization phase of the experiment.

C. EXPERIMENT SCENARIO

The experiment took place in a simulated urban environment of Vanves (a city situated 7.5 km south-west of Paris). The experiment's itinerary is shown in Fig. 6. The road consists of an on-street bicycle lane of 1.5 m in width with no separation between the cyclists and the motorized vehicles. Moderate traffic was generated in the same and opposite directions of the cyclist, and buses passed the cyclist from time to time. The participants were asked to ride the simulator for around 5 minutes to familiarize themselves with it (the virtual environment of the familiarization phase was different from the one used for this experiment). After the familiarization phase, we asked them to perform a simple task consisting of riding the bicycle for a short promenade (650 m) following the directional arrows painted on the bicycle lane until they reached the stop sign. The road geometry included two curves and three intersections. The cyclists were asked to turn right at the third intersection. The participants had full control over the different features of the simulator such as: handlebar, pedals, gears and brakes. The experiment lasted around 10 minutes, a duration which we deemed sufficient to test all the features of the simulator and to collect enough data for the post-analysis without exhausting the participants.

At the end of the experiment, the participants answered three questionnaires: The first one to collect general information about the participants and their cycling experience in real life and using the simulator; the second one was the Simulator Sickness Questionnaire (SSQ) [27]: with 16 questions to evaluate the occurrence of different symptoms during the experiment using a four-level scale (None, Slight, Moderate and Severe); and the third one was the NASA Task Load Index (TLX) [28], to evaluate the overall workload of the cycling task and the importance of each of the 6 work-load-factors under investigation, the participants evaluated each factor on a scale of 10 (1 for low and 10 for high, except for the performance where 1 for good and 10 for poor), then, it was converted to a 100-scale by multiplying by 10. The questionnaires were available both in English and French, as some participants only speak French.

FIGURE 6. The cycling track in the city of Vanves. Source: Google Maps

The trajectory and speed profile of one of the participants are shown in Fig. 7 and 8.

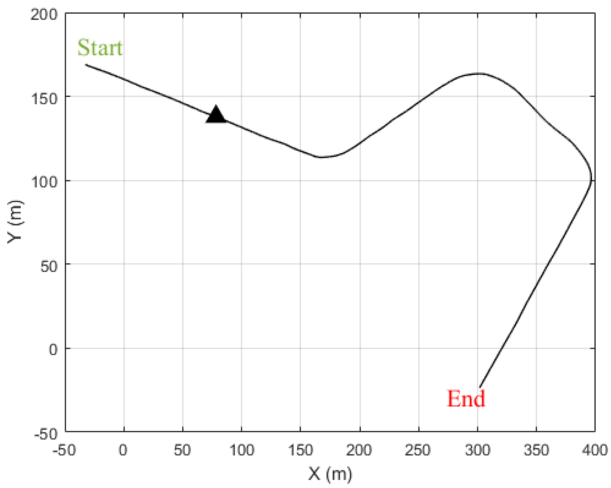

FIGURE 7. Trajectory of a participants due to the coordinate system of the virtual reality.

D. PHYSICAL VALIDITY

Several tests and scenarios were conducted at various speeds with the bicycle simulator. Sample results of the vertical displacement, side slip angle, lateral and longitudinal forces and rotational angles are presented in this section. The parameters of dynamic model of the bicycle were set to values from the literature [29] [30]. The stiffness and damping coefficients were taken from [31].

This article has been accepted for publication in a future issue of this journal, but has not been fully edited. Content may change prior to final publication. Citation information: DOI 10.1109/ACCESS.2021.3071214, IEEE Access

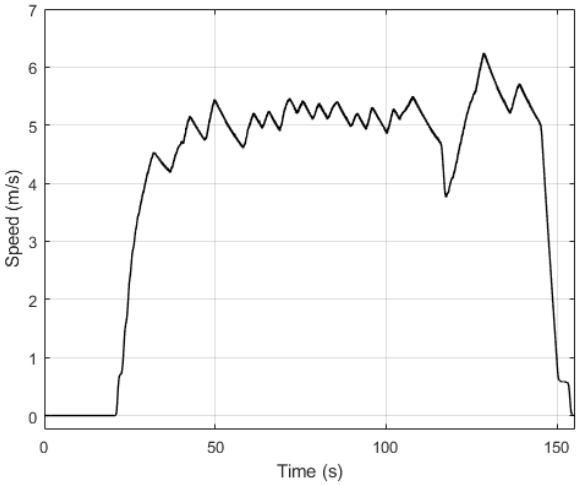

FIGURE 8. Speed profile of a participant.

1) Vertical displacement and force

The input for the longitudinal road profile was measured along an asphalt driving lane in a previous experiment conducted by IFSTTAR (see Fig. 9). The signal had a frequency of 1 kHz and a maximum amplitude of about $\pm$ 2.0 cm. A zoom on the time interval [20, 25] s shows the input signal in details. In order to reproduce the unevenness of the road surface we used a sinusoidal signal with random pulses as an input for the vibration actuators shown in Fig. 10.

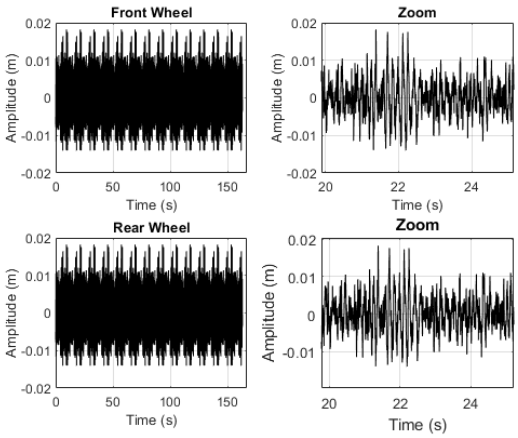

FIGURE 9. The road profile input under the front rear wheels, with zooms between 20 and 25 s.

Fig. 11, 12 and 13 show that the vertical displacement, the vertical acceleration and the vertical force of the front and rear wheels are influenced by the amplitude of the road profile (Fig. 9); this becomes clearer at the peaks and lows caused by the unevenness of the road profile between 22 and 23 s. We also notice that the vertical acceleration of the rear wheel is bigger than the front wheel due to the mass distribution (i.e. the rear wheel carries more weight than the front wheel).

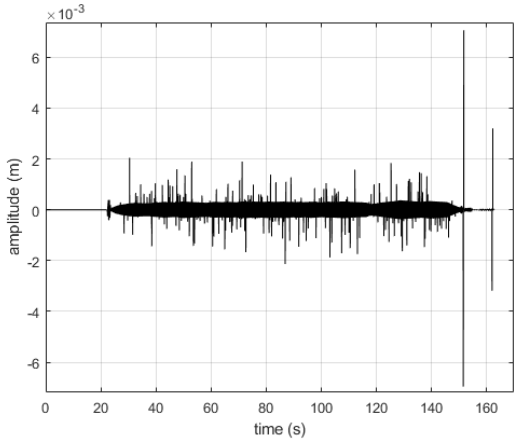

FIGURE 10. Actuators input.

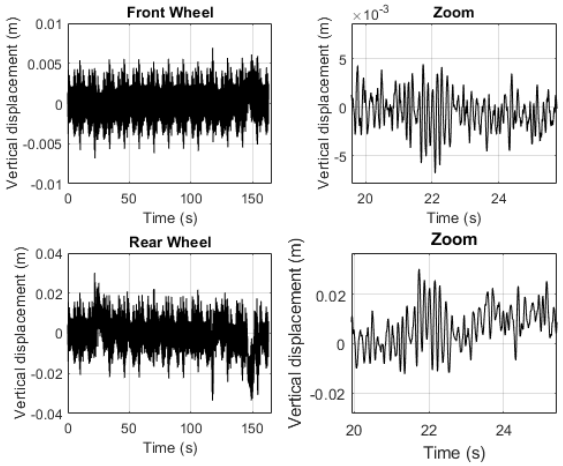

FIGURE 11. Vertical displacement estimation for the front and rear wheels, with zooms between 20 and 26 s.

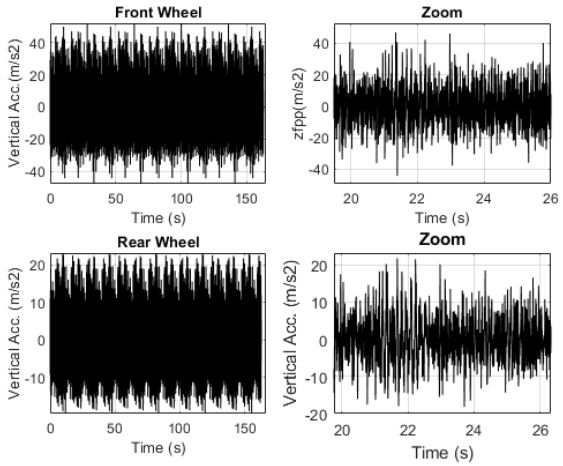

FIGURE 12. Vertical acceleration estimation for the front rear wheels with zoom between 20 and 26 s.

This article has been accepted for publication in a future issue of this journal, but has not been fully edited. Content may change prior to final publication. Citation information: DOI 10.1109/ACCESS.2021.3071214, IEEE Access

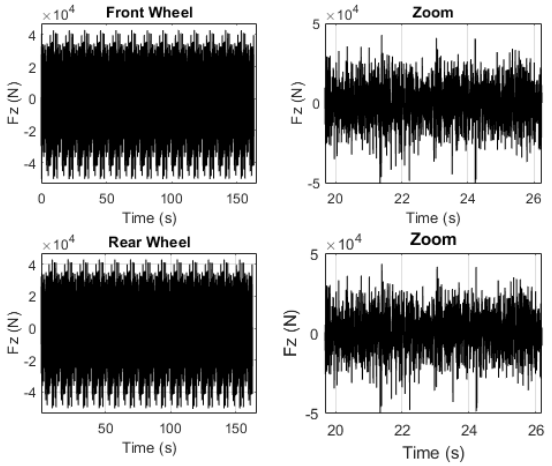

FIGURE 13. Vertical force for the front and rear wheels and zoom between 20 and 26 s.

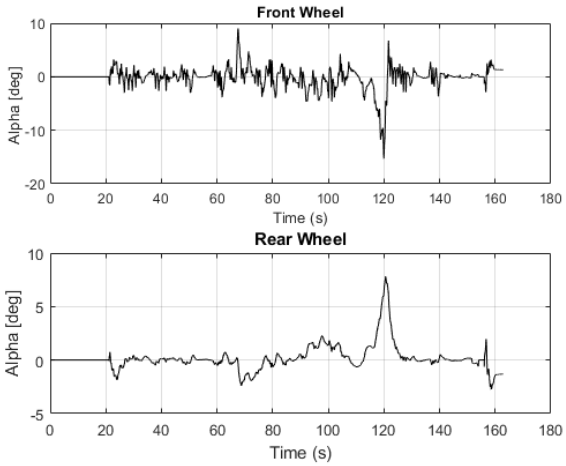

FIGURE 15. Side slip angle for the front and rear wheels.

2) Side slip angle and lateral force

Fig. 14 shows the steering angle and velocity measured and logged during one test using the incremental encoder. Fig. 15 shows the side slip angle of the front and rear wheels calculated using (5) and (6). The simulation results show the direct impact of the steering angle on the calculation of the side slip angle which becomes noticeable at the peak value of 120 s.

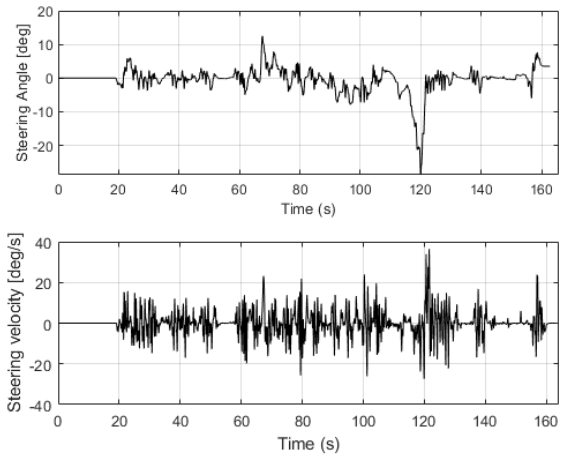

FIGURE 14. Steering angle and velocity of the bicycle simulator handlebar.

Fig. 16 shows the lateral position estimation of the bicycle simulator. The black line results from the former model where the lateral position was estimated depending on the coordinate system of the virtual reality, whereas the red line results from the new model where the lateral position was calculated using (11). The new model shows higher accuracy. This can be observed through the impact of the steering angle and velocity; especially around 70 and 120 s, where high values in steering angle result in substantial changes in the lateral position.

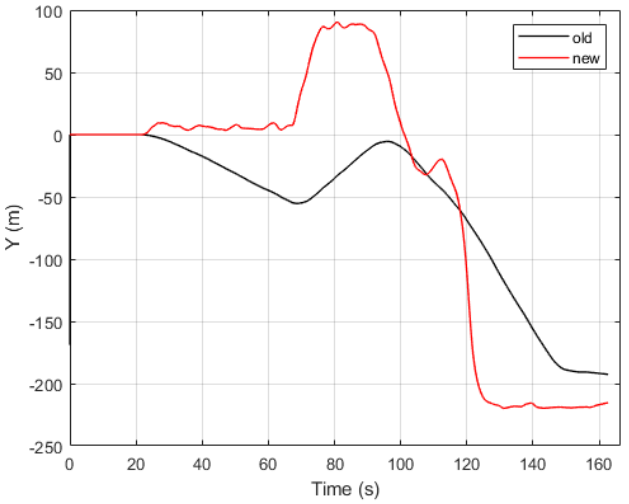

FIGURE 16. Lateral position estimation (m); the black line represents the former model and the red line represents the developed model.

Fig. 17 shows the lateral force of the front and rear wheels calculated using (9) and (10). The graph shows that the increase of the side slip angle causes an increase in the lateral force, this is particularly noticeable around 70, 100 and 120s.

3) Longitudinal force

During the simulation we used three different values of road adhesion coefficient to represent different surfaces and weather conditions. The longitudinal force shown in Fig. 19, which was calculated based on the adhesion coefficient in Fig. 18, shows the influence of different adhesion coefficients. For example, when the road surface is dry ($\mu = 0.8$) the longitudinal friction force peaks, whereas a wet surface ($\mu = 0.2$) results in a low longitudinal friction force.

4) Roll angle

Fig. 20 shows the simulation output for the roll angle. As noticed, the roll angle runs similarly to the steering angle as

This article has been accepted for publication in a future issue of this journal, but has not been fully edited. Content may change prior to final publication. Citation information: DOI 10.1109/ACCESS.2021.3071214, IEEE Access

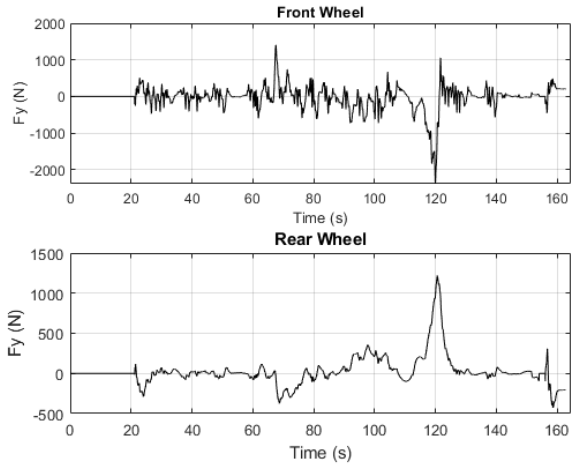

FIGURE 17. Lateral force of the front and rear wheels (N).

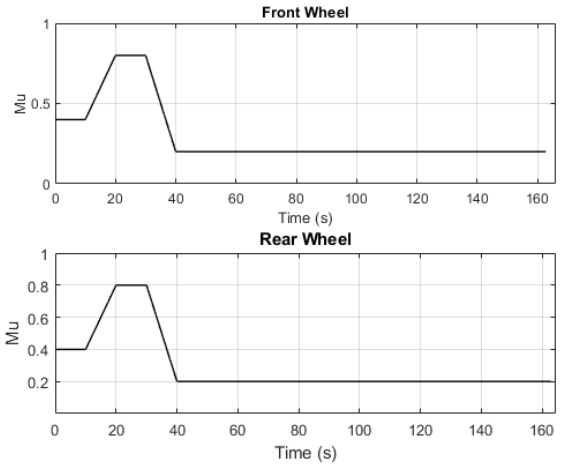

FIGURE 18. Adhesion coefficient input for the front and rear wheels of the bicycle simulator.

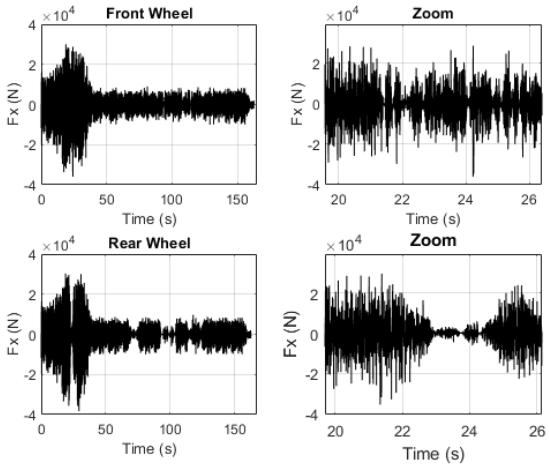

FIGURE 19. Longitudinal Force (N) for the front and rear wheel.

the increase of the steering angle implies a decrease of the radius of curvature. This effect of steering angle and radius of curvature is also noticed in roll speed and acceleration shown in Fig. 21 and 22. In the former model, the roll angle acceleration was calculated using the second derivative of the roll angle, whereas the new model calculates the roll angle acceleration using (19). Fig. 22 compare the outputs of the former and new models, it shows the improvement brought by the new model regarding accuracy and noise removal.

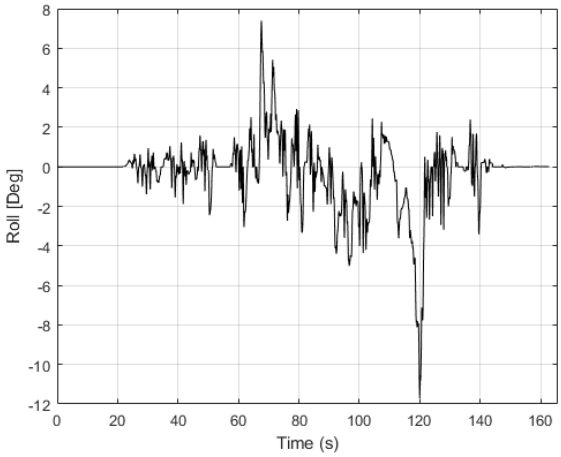

FIGURE 20. Roll angle.

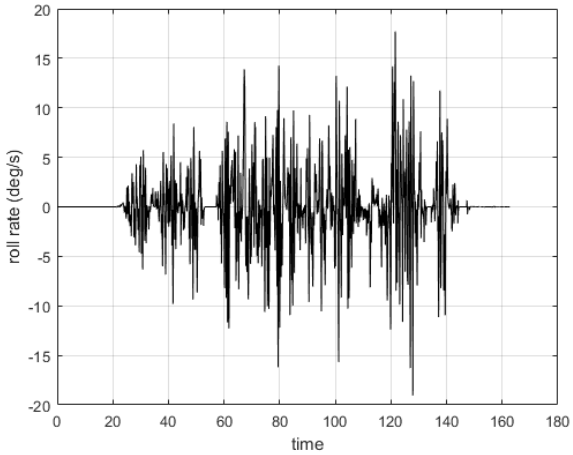

FIGURE 21. Roll rate .

5) Yaw angle

Fig. 23 shows the simulation output of the yaw angle, we notice the direct effect of the lateral position (Fig. 11) on yaw angle calculation. Yaw rate and acceleration are shown in Fig. 24 and 25. In the former model, yaw angle acceleration was calculated using the second derivative of the yaw angle, whereas the new model calculates the Yaw acceleration using (17). By comparing the results of the old and the new model

This article has been accepted for publication in a future issue of this journal, but has not been fully edited. Content may change prior to final publication. Citation information: DOI 10.1109/ACCESS.2021.3071214, IEEE Access

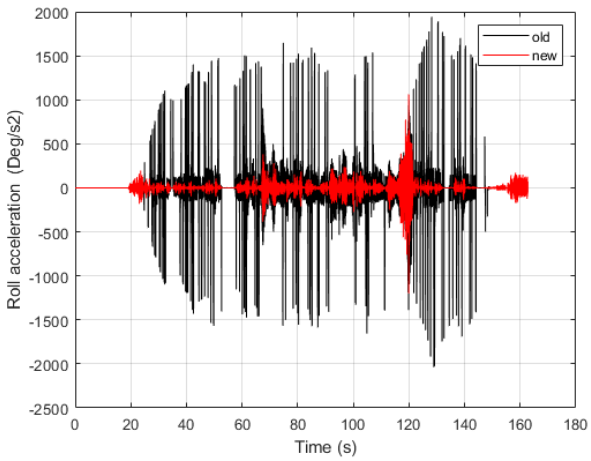

FIGURE 22. Comparison between roll acceleration values for the former and new models.

(Fig. 25) we notice the improvement brought by the new model regarding accuracy and noise removal.

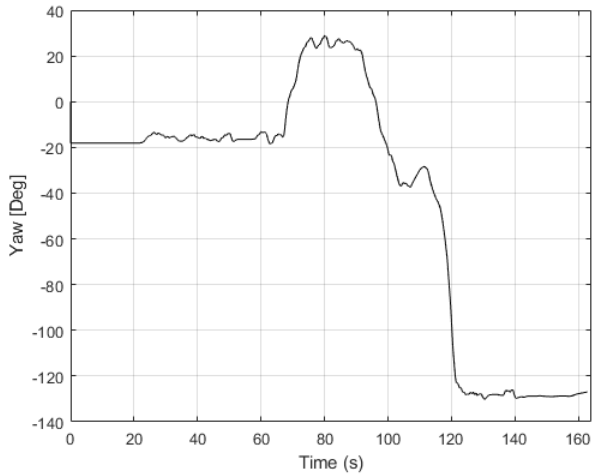

FIGURE 23. Yaw angle.

6) Pitch angle

The simulation output of the pitch rotation angle, rate and acceleration are shown in Fig. 26, 27 and 28. The small values could be explained by cycling on a flat surface which has minor impact on the pitch angle. An increase of the pitch angle could be noticed in acceleration and breaking phases. By comparing results between the previous and the new model (Fig. 28) we see the advantages of the new model regarding accuracy and noise removal.

E. SUBJECTIVE VALIDITY

The analysis of the first questionnaire shows that 7 of the participants had participated in a previous experiment using the same bicycle simulator before the recent improvement [1]. 8 of them declared sensitivity to motion sickness; 5

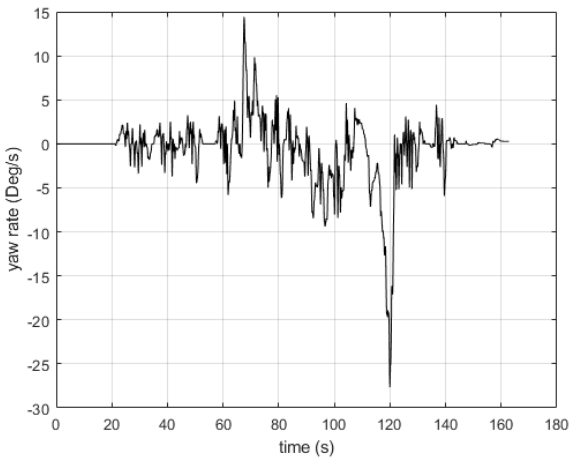

FIGURE 24. Yaw rate.

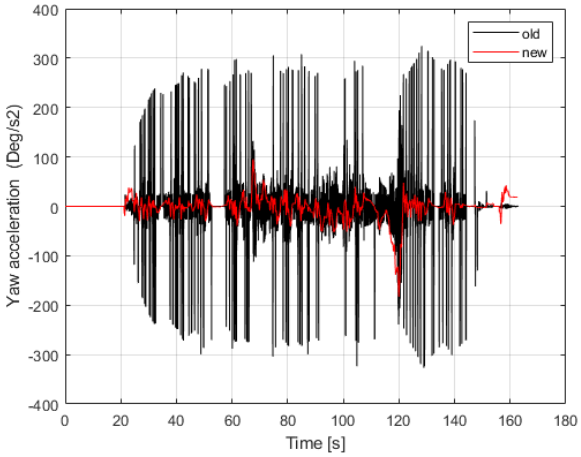

FIGURE 25. Comparison between yaw acceleration values for the former and new models.

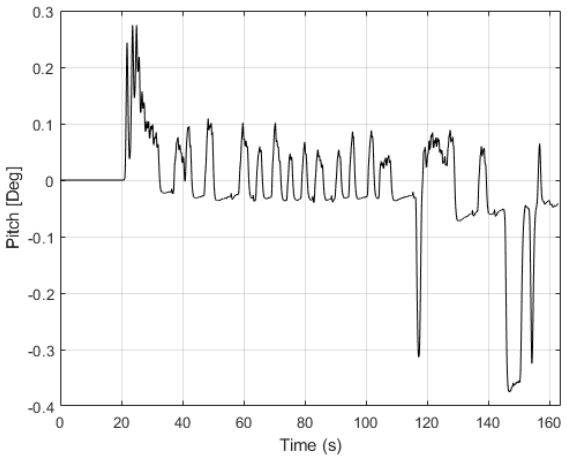

FIGURE 26. Pitch angle.

of them when reading during travelling. On evaluating the

This article has been accepted for publication in a future issue of this journal, but has not been fully edited. Content may change prior to final publication. Citation information: DOI 10.1109/ACCESS.2021.3071214, IEEE Access

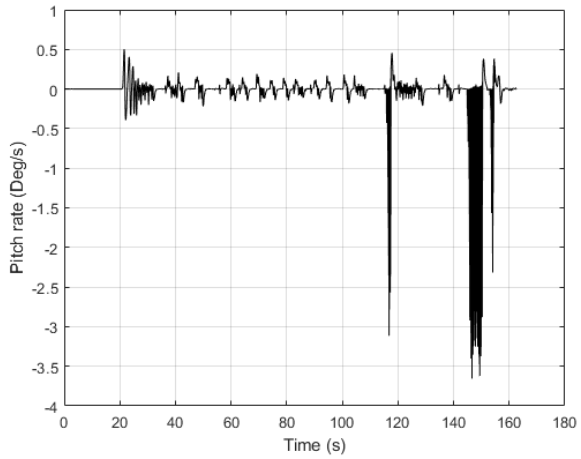

FIGURE 27. Pitch rate.

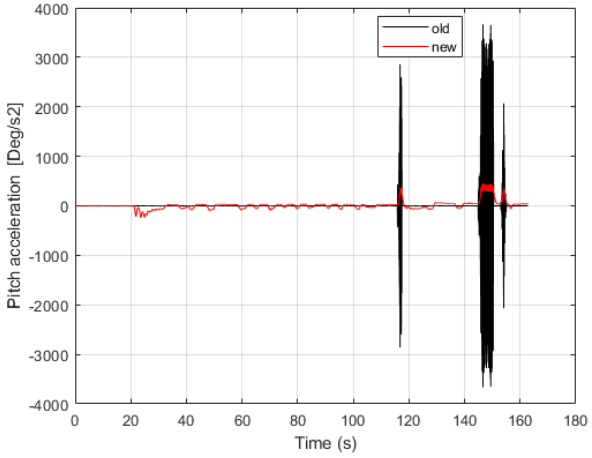

FIGURE 28. Comparison between pitch acceleration values for the former and new models.

realism of the simulator (compared to riding a real bicycle) the participants rating ranges between 3 and 9 on scale of 10 (mean=6.74, SD=1,57). This shows an improvement of the simulator compared to a previous experiment, where the participants evaluated the simulator with 6.1/10 [2]. The physical feeling of cycling, the design of the virtual road, traffic generation and other sensory cues, such as wind and the sound of the passing traffic were mentioned as the most realistic aspects of the simulator. However, some of the participants mentioned lacking the effect of the body posture when turning. This is because turning in the virtual reality is only affected by the steering angle and the body posture has no effect. The complete answers to the first questionnaire are shown in Appendix B.

Table 1 summarizes the results of NASA TLX questionnaire for the 36 participants. The first column shows the scales under assessment, the second column represents the average weight of each scale according to the personal opinion of each participant. This was calculated by answering 15 questions in which the scorer chose between two scales according to their importance. The weight of each scale is the number of times it was chosen. The third column is the average raw rating taken from the TLX questionnaire; and the last column represents the adjusted weighting, which is the multiplication of the weight and raw rating of each factor.

TABLE 1. Weighted rating of TLX questionnaire. The overall workload (OW)= mean of weighted ratings.

Scale title	Weight	Raw Rating	Adjusted rating
Mental Demand	3.13	45.56	142.61
Physical Demand	2.35	45.28	106.30
Temporal Demand	2.26	40.83	92.32
Performance	3.35	22.50	75.33
Effort	2.17	44.44	96.62
Frustration	1.74	24.17	42.03
Overall workload		37.13	92.53

The raw rating results show that the simulator requires intermediate mental/physical/temporal demand and effort. This is explained by the effort and concentration required when riding any bicycle and interacting with traffic since it is an active transport mode.

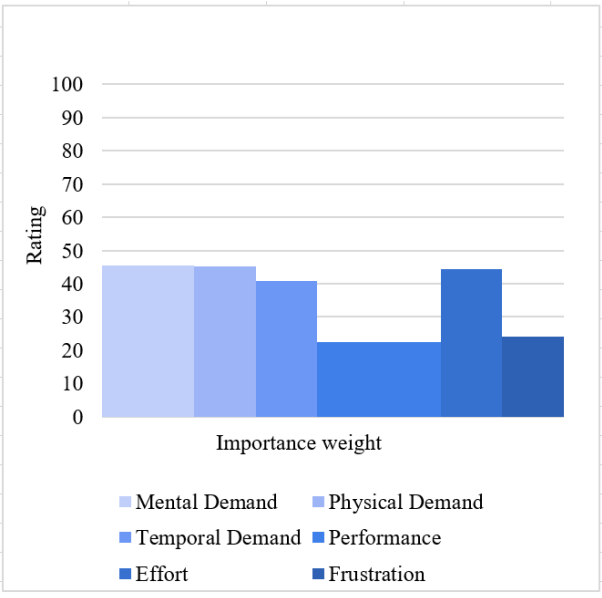

FIGURE 29. Nasa Task Load Index analysis results: Weighted work load score. The width of each column represents the importance weight of each factor.

Fig. 29 compares the weighted average of each workload scale. It can be seen that the performance factor received a relatively low rating but a high importance, whereas the frustration factor received an intermediate rating but a low importance (meaning that the task was simple and easy to accomplish), so that both factors contribute in the similar amounts to the overall workload.

The analysis of the simulator sickness questionnaire listed in Table 2 shows that the average total severity for all partici-

This article has been accepted for publication in a future issue of this journal, but has not been fully edited. Content may change prior to final publication. Citation information: DOI 10.1109/ACCESS.2021.3071214, IEEE Access

pants is 14.65. By comparing this result to the possible scores listed in Table 3, we see that the total severity of the simulator is slight (less than 78.5).

TABLE 2. Simulator Sickness Questionnaire Results.

	Nausea	Oculomotor	Disorientation	Total Severity
mean	10.86	14.32	12.37	14.65
SD	18.25	14.26	19.2	17.58
min	0	0	0	0
max	57.24	37.9	41.76	52.36

TABLE 3. Possible results of the Simulator Sickness Questionnaire.

	Nausea	Oculomotor	Disorientation	Total Severity
none	0	0	0	0
slight	66.8	53.1	97.4	78.5
moderate	133.6	106.1	194.9	157.1
severe	200.3	159.2	292.3	235.6

Fig. 30 contains the score distribution obtained from the 36 participants. It can be seen that 6 participants (17 %) reported no symptoms from their exposure to the simulator, and the rest reported slight symptoms of simulator sickness (less than 78.5),

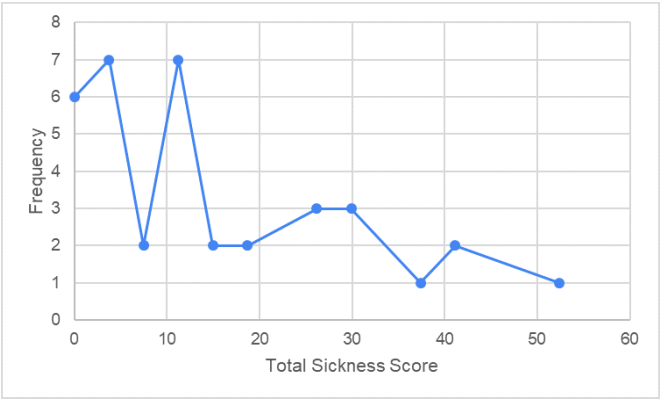

FIGURE 30. Frequency distribution of total sickness scores (N=36).

Fig. 31 shows that the average severity of all symptoms is slight (less than 1), with a slight increase in the general discomfort, which could be explained by the exposure to the virtual reality displays.

Fig. 32 shows that males experienced an increase of eye strain, whereas females experienced an increase in difficulty focusing.

Fig. 33 shows that participants with corrected vision experienced higher symptoms in general discomfort and fatigue, whereas normal vision participants experienced more eye strain and difficulty focusing.

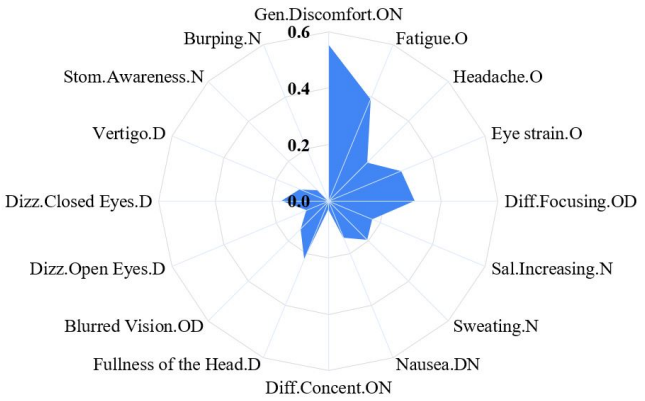

FIGURE 31. Mean scores observed in each item of the exposure of simulator sickness questionnaire. The O, D and N letters following the name of each item indicate in which class(es) of symptoms the corresponding item was involved: O corresponds to Oculomotor discomfort, D to Disorientation and N to Nausea.

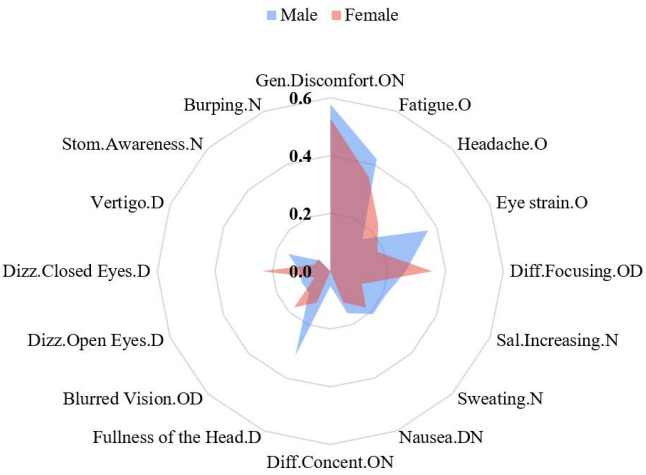

FIGURE 32. Mean scores observed in each item of the simulator sickness questionnaire during the experiment. (a) Men (blue area) and women (red area). The O, D and N letters following the name of each item indicate in which class(es) of symptoms the corresponding item was involved: O corresponds to Oculomotor discomfort, D to Disorientation and N to Nausea.

IV. CONCLUSION AND FUTURE WORK

In this paper, we proposed an original mathematical model of bicycle dynamics which was experimentally validated on an immersive bicycle simulator at various speeds and different cycling maneuvers. The developed model deals with 6 degrees of freedom (longitudinal, lateral, vertical, Yaw, Pitch and Roll). The main advantages of the model are its simplicity, compatibility with the bicycle simulator, and its ability to be applied to a real bicycle.

The inputs of the model, such as steering angle, pedaling and braking were measured and logged in real time. Their influence on vertical, lateral and longitudinal forces, velocities and displacements were observed. The comparison between the previous mathematical model and the model discussed in this paper shows that the proposed model produces more accurate estimations. Improvements were noticed in

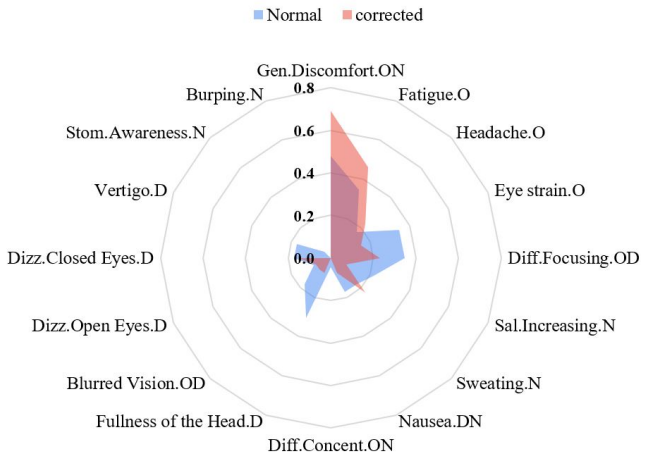

FIGURE 33. Mean scores observed in each item of the simulator sickness questionnaire during the experiment. (a) normal vision (blue area) and corrected-to-normal vision (red area). The O, D and N letters following the name of each item indicate in which class(es) of symptoms the corresponding item was involved: O corresponds to Oculomotor discomfort, D to Disorientation and N to Nausea.

the following areas: the compatibility of the lateral position with the trajectory and yaw angle, the noise removal when calculating yaw, pitch and roll accelerations, the impact of the unevenness of the road profile on the vertical displacement and force, the steering angle effect on the side slip angle, lateral displacement and yaw, and the effect of road adhesion on the longitudinal force.

The analysis of the simulator sickness questionnaire shows a drop in the severity of the simulator (TS =14.65) compared to the old experiment (TS= 32.54). This could be explained by using more realistic virtual reality which affected (alongside the installment of the actuators and the asphalt specimen) the subjective evaluation of the realism of the simulator increased from 6.1 to 6.74/10.

The validity of the bicycle simulator allows us to safely cyclists' behavior in risky situations and analyze their reactions and interactions with different features of the infrastructure such as, radius of curvature, intersections and lateral and longitudinal slopes. In future work, we will conduct real life experiments using an instrumented bicycle in different locations and countries, particularly Sweden and Spain, in order to compare the output from the developed algorithms on the simulator with the road and to test the robustness of the proposed approach.

V. ACKNOWLEDGEMENTS

The authors gratefully acknowledge the contributions of: Transportation Infrastructures section of the Department of Civil, Chemical, Environmental and Materials Engineering (DICAM) at University of Bologna for designing and casting the asphalt specimen used to simulate road surface; and SimTeam represented by Stephane Caro for installing the actuators and the assistance during the preparation of the experiment.

REFERENCES

[1] M. Shoman and H. Imine, "Modeling and simulation of bicycle dynamics," in TRA 2020, Transportation Research Arena, TRA, 2020.
[2] M. Shoman and H. Imine, "Subjective validity of bicycle simulators," in Proceedingd, VEHICULAR 2020 : The Ninth International Conference on Advances in Vehicular Systems, Technologies and Applications, October 2020, Porto, Portugal, 2020.
[3] W. H. Organization et al., Global status report on road safety 2018. World Health Organization, 2018.
[4] A. Billot-Grasset, E. Amoros, and M. Hours, "How cyclist behavior affects bicycle accident configurations?," Transportation research part F: traffic psychology and behaviour, vol. 41, pp. 261–276, 2016.
[5] O. national Interministériel de la sécurité routière, La sécurité routière en France Bilan de l'accidentalité de l'année 2017. Observatoire national Interministériel de la sécurité routière, 2017.
[6] M. M. Haddak, "Exposure-based road traffic fatality rates by mode of travel in france," Transportation research procedia, vol. 14, pp. 2025–2034, 2016.
[7] I. T. Forum, Cycling Safety Summary and Conclusions. Organisation for Economic Co-operation and Development OCED, 2018.
[8] N. Ghasemi, H. Imine, A. Simone, C. Lantieri, V. Vignali, and K. Finamore, "Longitudinal motion cueing effects on driver behaviour: a driving simulator study.," Advances in transportation studies, vol. 49, 2019.
[9] A. Owczarkowski, D. Horla, P. Kozierski, and T. Sadalla, "Dynamic modeling and simulation of a bicycle stabilized by lqr control," 2016 21st International Conference on Methods and Models in Automation and Robotics (MMAR), pp. 907–911, 2016.
[10] Q. He, X. Fan, and D. Ma, "Full bicycle dynamic model for interactive bicycle simulator," Journal of Computing and Information Science in Engineering, vol. 5, no. 4, pp. 373–380, 2005.
[11] F. J. Whipple, "The stability of the motion of a bicycle," Quarterly Journal of Pure and Applied Mathematics, vol. 30, no. 120, pp. 312–321, 1899.
[12] U. Kiencke and L. Nielsen, "Automotive control systems: for engine, driveline, and vehicle," 2000.
[13] G. Dialynas, R. Happee, and A. L. Schwab, "Design and hardware selection for a bicycle simulator," Mechanical Sciences, vol. 10, no. 1, pp. 1–10, 2019.
[14] D.-S. Kwon, G.-H. Yang, C.-W. Lee, J.-C. Shin, Y. Park, B. Jung, D. Y. Lee, K. Lee, S.-H. Han, B.-H. Yoo, et al., "Kaist interactive bicycle simulator," in Proceedings 2001 ICRA. IEEE International Conference on Robotics and Automation (Cat. No. 01CH37164), vol. 3, pp. 2313–2318, IEEE, 2001.
[15] D.-S. Kwon, G.-H. Yang, Y. Park, S. Kim, C.-W. Lee, and J.-C. Shin, "Kaist interactive bicycle racing simulator" the 2nd version with advanced," IEEE/RSJ International Conference on Intelligent Robots and Systems, 2002.
[16] C.-K. Chen, F.-J. Chen, J.-T. Huang, and C.-J. Huang, "Study of interactive bike simulator in application of virtual reality," Journal of the Chinese society of mechanical engineers, vol. 28, no. 6, pp. 633–640, 2007.
[17] S. V. Babu, T. Y. Grechkin, B. Chihak, C. Ziemer, J. K. Kearney, J. F. Cremer, and J. M. Plumert, "An immersive virtual peer for studying social influences on child cyclists' road-crossing behavior," IEEE transactions on visualization and computer graphics, vol. 17, no. 1, pp. 14–25, 2011.
[18] S. 'e. p. Caro, N. Chaurand, N.-T. Dang, and F. Vienna, "Design of a traffic simulator for the study of the behavior of cyclists," Journal of Transport - Dissemination (JTD) of the Scientific and Technical Network, 2013.
[19] S. Caro and S. Bernardi, "The role of various sensory cues in self-speed perception: a bicycle riding simulator preliminary study," in DSC 2015-Driving simulation conference, 2015.
[20] S. Caro, F. Vienne, N. Chaurand, N.-T. Dang, S. Bernardi, and B. Ramdani, "Un simulateur de îlo pour de nouvelles recherches," in Géri Vélo-IFSTTAR, p. 29p, 2015.
[21] A. Simone, V. Vignali, and M. Shoman, "Looking behavior to vertical road signs on rural roads," MOJ Civil Engineering, vol. 4, no. 4, 2018.
[22] A. Bucchi, C. Sangiorgi, and V. Vignali, "Traffic psychology and driver behavior," Procedia-social and behavioral sciences, vol. 53, pp. 972–979, 2012.
[23] G. Dondi, V. Vignali, C. Lantieri, and G. Manganelli, "Effects of flickering seizures on road drivers and passengers," Procedia-social and behavioral sciences, vol. 53, pp. 711–720, 2012.
[24] H. Imine, Observation d'états d'un véhicule pour l'estimation du profil dans les traces de roulement. PhD thesis, Versailles-St Quentin en Yvelines, 2003.

[25] H. Imine, L. Fridman, H. Shraim, and M. Djemai, Sliding mode based analysis and identification of vehicle dynamics, vol. 414. Springer Science & Business Media, 2011.
[26] P.-M. Damon, Estimation pour le développement de systèmes d'aide à la conduite des véhicules à deux-roues motorisés. PhD thesis, 2018.
[27] R. S. Kennedy, N. E. Lane, K. S. Berbaum, and M. G. Lilienthal, "Simulator sickness questionnaire: An enhanced method for quantifying simulator sickness," The international journal of aviation psychology, vol. 3, no. 3, pp. 203–220, 1993.
[28] S. G. Hart, "Nasa task load index (tlx). volume 1.0; computerized version," 1986.
[29] J. K. Moore, M. Hubbard, J. Kooijman, and A. Schwab, "A method for estimating physical properties of a combined bicycle and rider," in ASME 2009 international design engineering technical conferences and computers and information in engineering conference, pp. 2011–2020, American Society of Mechanical Engineers, 2009.
[30] J. K. Moore, M. Hubbard, A. L. Schwab, and J. D. Kooijman, "Accurate measurement of bicycle parameters," in Proceedings, Bicycle and Motorcycle Dynamics 2010 Symposium on the Dynamics and Control of Single Track Vehicles, 20Ű22 October 2010, Delft, The Netherlands, 2010.
[31] V. E. Bulsink, A. Doria, D. van de Belt, and B. Koopman, "The effect of tyre and rider properties on the stability of a bicycle," Advances in mechanical engineering, vol. 7, no. 12, p. 1687814015622596, 2015.

MURAD M. SHOMAN received the B.S. degree in civil engineering from An-Najah National University, Nablus, Palestine, in 2013 and the M.Sc. in civil engineering from University of Bologna, Bologna, Italy, in 2016. He is currently pursuing the Ph.D. in transportation engineering at Gustave Eiffel University, Champs sur Marne, France. From 2016 to 2019, he was a technical instructor at the civil engineering department in Ramallah Triaing Center, Ramallah, Palestine and a part-time lecturer at civil engineering department in Palestine Polytechnic University, Hebron, Palestine.

His research interests include active Transportation modes, bicycle modeling and stability, road safety and road-users' behavior. He published 3 papers. Mr. Shoman's awards include Erasmus Mundus grant and Marie Skłodowska-Curie Actions grant.

HOCINE IMINE received the Master's and Ph.D. degrees in robotics and automation from Université de Versailles Saint-Quentin-en-Yvelines, Versailles, France, in 2000 and 2003, respectively, and the Accreditation to Supervise Research (Habilitation Diriger des Recherches, HDR) from the University of Valenciennes and Hainaut-Cambresis, Valenciennes, France, in 2012. In 2005, he joined IFSTTAR (University Gustave Eiffel), where he is currently a research director. He is Member of IFAC Technical Committee on Transportation systems (TC 7.4). He is Guest Editor of International Journal of Vehicle Design, Special Issue on: "Variable Structure Systems in Automotive Applications". He served as a Guest Editor for the International Journal of Vehicle Design Special Issue on Variable Structure Systems in Automotive Applications and member of Editorial Board of Journal of Advanced Transportation, Vehicles journal and International Journal of Automotive Innovation.

His research interests include Intelligent Transportation Systems, heavy vehicle modeling and stability, diagnosis, nonlinear observation, nonlinear control. He published 2 books, over 80 technical papers, and several industrial technical reports.

.

APPENDIX A DYNAMICAL AND MECHANICAL PARAMETERS OF THE BICYCLE SIMULATOR USED DURING THE SIMULATION

Parameter	Symbol	unit	value
Wheelbase	w	m	1.101
Mass of bicycle + rider	m	kg	85
Center of gravity (bicycle+rider)	COG	m	x= 0.291 , z=-1.09
Distace from COG to the center of rear wheel	l_r	m	0.293
Distace from COG to the center of front wheel	l_f	m	0.808
the horezental distance between $G_f and G_r$	K	m	0.614
the frontal surface for the bike and the cyclist body	S	m^2	0.4
coefficient of aerodynamic resistance	C_{ax}	%	0.824
Steer Axis tilt (caster angle)	ϵ	rad	0.367
trail	c	m	0.083
mass of the front part of the bike\rider	m_F	kg	23
Vertical tiffness	k	N/m	108000
Damping ratio	B	N.s/m	5448
Moment of inertia around x	I_{xGf}	kg.m^2	0.387
Moment of inertia around z	I_{zGf}	kg.m^3	0.167
Mass of the rear part of the bike\rider	m_R	kg	62
Moment of inertia around x	I_{xGR}	kg.m^2	11.96
Moment of inertia around z	I_{zGr}	kg.m^2	3.105
Wheel radii	r	m	0.35
Front tire lateral stiffness	C_y	N/m	490
front wheel moment of inertia around y axis	I_{Fyy}	kg.m^3	0.144

APPENDIX B PARTICIPANT RESPONSES TO THE GENERAL QUESTIONNAIRE ABOUT THEIR CYCLING EXPERIENCE

Participant Number	Age	Gender	Do you wear glasses ?	Do you wear lenses?	Cycling per month (km)	Cycling experience (years)	Previous experiment on a bicycle simulator	motion sickness	motion sickness symptoms
1	25	Female	No	No	20	20	No	No	-
2	26	Female	No	No	0	18	Yes	No	-
3	28	Female	No	No	0	23	No	No	-
4	26	Male	No	No	5	20	Yes	No	-
5	22	Female	No	No	0	10	No	No	-
6	40	Male	No	No	40	20	No	No	-
7	22	Male	No	No	40	15	No	Yes	nausea, in bus
8	25	Female	Yes	No	0	0	No	Yes	car motion sickness
9	21	Male	No	No	0	2	No	Yes	Stomach sickness
10	23	Male	No	No	400	16	No	No	-
11	23	Male	No	Yes	0	15	No	No	-
12	22	Male	Yes	No	40	15	No	No	-
13	21	Male	Yes	No	40	15	No	No	-
14	22	Male	Yes	No	20	18	No	No	-
15	25	Male	No	No	15	15	No	Yes	while reading in a vehicle
16	22	Female	No	No	20	14	No	No	-
17	50	Female	Yes	No	0	45	No	No	-
18	23	Female	No	No	0	0	No	No	-
19	29	Male	No	No	0	15	No	No	-
19	26	Female	Yes	No	0	18	No	No	-
21	30	Male	No	No	2.5	20	Yes	Yes	while reading in a vehicle
22	27	Male	No	No	8	21	Yes	No	-
33	26	Male	No	No	7	18	Yes	No	-
24	28	Male	No	No	40	20	No	No	-
25	26	Female	No	No	0	0	No	No	-
26	24	Female	Yes	No	0	0	No	No	-
27	69	Female	Yes	No	0	20	No	Yes	while reading in a vehicle
28	29	Female	Yes	No	5	23	No	No	while reading in a vehicle
29	26	Female	Yes	No	0	5	No	Yes	while reading in a vehicle
30	25	Female	No	Yes	8	17	Yes	No	-
31	27	Female	Yes	No	30	4	Yes	No	-
32	28	Male	No	No	0	3	No	No	-
33	23	Male	No	No	0	0	No	No	-
34	32	Female	No	No	0	22	No	No	-
35	25	Male	No	No	0	7	No	No	-
36	35	Female	No	No	0	29	No	No	-
mean	27.81	18M/18F	11 yes	2 yes	20.57	14.53	7 yes	7 yes	-
SD	9.01	-	-	-	66.62	9.62	-	-	-
min	21	-	-	-	0	0	-	-	-
max	69	-	-	-	400	45	-	-	-

This article has been accepted for publication in a future issue of this journal, but has not been fully edited. Content may change prior to final publication. Citation information: DOI 10.1109/ACCESS.2021.3071214, IEEE Access

A. APPENDIX B (CONTINUED)

Participant Number	Realism of the simulator	the most realistic aspects	features to be improved
1	9	buildings and cars	the streets
2	8	Souds, physical effects, virtual environment	Virtual picture when turning the bicycle
3	5	the setting on the screen	the bicycle should be more constrained to the soil
4	7	The driving of the bicycle itself, like the physical implication and muscle memory you put in the driving.	The realism of the environment - The fact that you when you turn, you should lean on the side you're turning- a lot or a bit, depending on your speed and the angle of the turn.
5			
6			
7			
8			
9	8	Cars coming into the bike lane	
10			
11	7	The pedaling and wind action	An ability for the bike to lean in turns
12	6	The apparatus (the bike and the components)	Processing speed. There was a delay in seeing ones action getting translated onto the screen.
13	7	The bicycle itself including turning maneuvers	The sense of speed
14			
15	7	The true feel that you get while cycling at a real road. The bicycle simulator did a great job, but somehow I felt that I didn't that feel of anxiousness that you get while cycling at areal road with real traffic.	May be having some kind of a virtual environment which can give a actual feel of cycling on a road.
16	7	Airflow from fans, road resistance	Feeling of turning
17	9	Movement of scenery around me	Reaction of bus behind the cyclist to avoid flattening him/her.
18			
19	7	For sure the feeling of riding the bike as it was real and also the road in front of you.	The air dynamics as while we are riding in real the air motion surrounding us is different.
19	5	The bike was real.	The connection between the bike and the road. I don't feel like I can control the path of my bike very well.
21	5	le fait de pouvoir voir à gauche, droite et derrière, le vélo, la ventilation (bien qu'un peu forte)	j'ai eu l'impression d'être lent à l'écran alors que je pédalais vite
22	8	pedaling	breaking, scenarios and perceived speed
33			
24	7	The roads with the ground lines, traffic lights/signs and so on.	The behavior of the buses/cars as they disregard cyclists and can drive-by too close to the cyclist.
25			
26	3	the road evolution	
27	7	Cycling on a real bicycle, feeling of the "wind" blowing, the danger of cycling along a busy street, seeing the shops go by	There should be more pedestrians walking along the streets, perhaps other cyclists on the lane.
28	8	The acceleration and break systems	The part I was most uncomfortable with was because it was fixed in a way I could not feel the gravity acting when I stop or the natural inclination the bicycle does when I turn right or left, for example.
29	4	the road evolution	Perhaps, the part with the bycicle
30	5		More cars, people crossing the street or traffic light.
31	8		
32			
33			
34			
35			
36	8	Cars	More sound
mean	6.74		
SD	1.57		
min	3		
max	9		